



## Changing active sites in Cu–CHA catalysts: deNO<sub>x</sub> selectivity as a function of the preparation method

Upakul Deka<sup>a,b</sup>, Ines Lezcano-Gonzalez<sup>a,b</sup>, Stewart J. Warrender<sup>c</sup>, A. Lorena Picone<sup>c</sup>, Paul A. Wright<sup>c</sup>, Bert M. Weckhuysen<sup>b</sup>, Andrew M. Beale<sup>b,\*</sup>

<sup>a</sup> Materials innovation institute (M2i), Mekelweg 2, 2628 CD Delft, The Netherlands

<sup>b</sup> Inorganic Chemistry and Catalysis Group, Debye Institute for Nanomaterials Science, Utrecht University, Universiteitsweg 99, 3584 CA, Utrecht, The Netherlands

<sup>c</sup> EaStCHEM School of Chemistry, University of St. Andrews, Purdie Building, North Haugh, St. Andrews, Fife KY16 9ST, UK

### ARTICLE INFO

#### Article history:

Available online 8 May 2012

#### Keywords:

NH<sub>3</sub>–SCR

Cu–SSZ-13

Cu–SAPO-34

CVD–IE

Active sites

### ABSTRACT

The selective catalytic reduction of NO<sub>x</sub> with ammonia (NH<sub>3</sub>–SCR) has been studied over Cu–CHA catalysts in which the loading of copper species was achieved using three different synthetic routes: two are based on post-synthetic treatment of the zeolite material (via aqueous or vapor phase) and a third involves the direct synthesis of a Cu-loaded SAPO-34. The catalysts were subsequently characterized by XRD, solid-state NMR, UV–vis and XAFS spectroscopies. Whilst the catalysts prepared via wet chemical routes show excellent deNO<sub>x</sub> activity and high selectivity to N<sub>2</sub>, the one prepared via chemical vapor deposition gave the undesired product N<sub>2</sub>O in significant quantities. Isolated mononuclear Cu<sup>2+</sup> ions in the vicinity of six-membered rings (6mrs, part of the *d6r* sub-units of CHA) were found to be active sites in both catalysts prepared via the wet chemical approaches. In contrast, XAFS data revealed that the catalyst prepared via chemical vapor deposition possesses Cu in two different environments: isolated Cu<sup>2+</sup> cations and CuAlO<sub>2</sub>-type species. Catalytic experiments revealed a strong correlation between the number of isolated mononuclear Cu<sup>2+</sup> in or near the plane of the 6m rings and N<sub>2</sub> production, whereas the presence of CuAlO<sub>2</sub> species appears to promote the formation of undesired N<sub>2</sub>O.

© 2012 Elsevier Inc. All rights reserved.

### 1. Introduction

Growing environmental concerns and subsequent stringent legislative regulation over the past two decades have resulted in the need to find innovative ways to deal with exhaust emissions in mobile applications. Ammonia-Selective Catalytic Reduction (NH<sub>3</sub>–SCR) has been realized as an effective technology for the reduction of NO<sub>x</sub> gases present in the exhaust of heavy duty diesel vehicles. Since first reported by Iwamoto et al., Cu-containing zeolites have been investigated as efficient catalysts in this reaction [1]. In particular, zeolites such as ZSM-5 (MFI structure), MOR, FAU and BEA (see <http://www.iza-structure.org/databases> for more information) have received much attention from both academia and industry [2,3]. However, these zeolites have been rarely applied in commercial applications due to their lack of both hydrothermal stability and low temperature activity. Recent studies have shown Cu–CHA to be an efficient catalyst under relevant SCR conditions [4,5]. The exceptional low temperature activity, high N<sub>2</sub> selectivity and high hydrothermal stability makes Cu–CHA one of the most promising catalysts expected to meet with future needs.

A recent study by Fickel et al. using Rietveld refinement of synchrotron-based powder X-ray diffraction (XRD) data revealed an exclusive occupation of Cu<sup>2+</sup> cations in the plane of the six-ring that comprise each end of the double six membered ring (*d6r*) sub-units of SSZ-13 (CHA structure) [6,7]; in comparison Cu–ZSM-5 is known to possess 5 cationic positions for Cu<sup>2+</sup> within its framework [8]. EXAFS data further revealed that the Cu<sup>2+</sup> ions do not sit in the center of the plane of the six-ring but rather tend to be displaced towards the edge of the ring in a 3–4 coordinate planar arrangement [5]. Recent in situ UV–vis and combined XAFS/XRD studies confirmed that such species remain intact during NH<sub>3</sub>–SCR and are thus responsible for the high catalytic activity [5,9]. A similar conclusion has recently been put forward for the high activity of Fe–BEA systems for the same reaction, the active species being proposed to be monomeric Fe<sup>3+</sup> species [10].

The difference between previous attempts to elucidate active sites in the NH<sub>3</sub>–SCR reaction and this particular case was the use of the CHA zeolite [3,11]. Owing to the tendency of Cu ions to be located almost exclusively at one crystallographic position in the CHA structure, determination of the active site becomes easier when compared to a zeolite with multiple cationic positions (e.g. in ZSM-5) or in a system with propensity for the Cu ions to ‘cluster’. The studies described above showed for the first time that

\* Corresponding author.

E-mail address: [a.m.beale@uu.nl](mailto:a.m.beale@uu.nl) (A.M. Beale).

the isolated location of  $\text{Cu}^{2+}$  in the double six rings was responsible for the high SCR activity exhibited by Cu-CHA type materials.

The current work shows the effect of preparation methods on the type of Cu species formed within CHA structures. Three different preparation methods for producing Cu ion-exchanged microporous materials are compared: (a) conventional wet ion exchange preparation of Cu-SSZ-13; (b) chemical vapor deposition of Cu ions within SSZ-13; and (c) direct synthesis of a Cu-loaded SAPO-34 material in which the Cu species occupy extra-framework cation sites. The principle aim of this study was to compare the tendency of the synthetic methods to create the unique Cu environments previously observed to be active for  $\text{NH}_3$ -SCR. Conventional wet ion exchange is a widely used technique to exchange metal ions into zeolites. However, problems such as formation of extra framework metal species owing to over-exchange of the metal salt, or metal clustering is known to occur in such bottom-up, wet approaches [12]. Chemical vapor deposition (CVD), on the other hand, is a top-down approach used commonly in the semiconductor industry to create metal-layers on a flat substrate. However, upon careful choice of metal salt, reactor system and flow conditions, one can also expect to create single metal sites within a porous support structure [12]. Chemical vapor deposition ion exchange using  $\text{CuCl}$  as the metal salt has previously been employed by either using a vacuum controlled approach to load a ZSM-5 wafer or under inert conditions to load zeolite Y with Cu [13–15]. Well dispersed Cu species within the zeolite were successfully obtained in these cases. Finally a direct synthetic approach towards Cu-SAPO-34 was used: this enabled comparison of Cu SSZ-13 to a catalyst with a similar CHA framework structure but prepared via an alternative method. This general approach was reported by Picone et al. for the inclusion of copper cyclam complexes as templates in the SAPO STA-7 (closely related to the SAPO-34 structure). Calcination then releases the  $\text{Cu}^{2+}$  cations into extra-framework, charge-balancing sites [16]. This approach for the inclusion of  $\text{Cu}^{2+}$  obviates the need for an additional aqueous cation exchange step, which has previously been used to generate Cu-SAPO-34 catalysts, [17,18], but which can lead to framework damage, especially for aluminophosphates. Here we describe the analogous use of the copper complex Cu-triethylenetetramine as a structure directing agent (SDA) for direct synthesis of Cu-SAPO-34, with subsequent calcination to give a copper-loaded Cu-SAPO-34 catalyst. Two comparable direct synthesis incorporations of copper cations in CHA have recently been reported for Cu-SAPO-34 (using morpholine [19] – for which the products were not fully characterized) and for the zeolite Cu-SSZ-13 (using copper-tetraethylenepentamine [20]), each of which is active for  $\text{NH}_3$  NO SCR. Although the Cu-complex-templated Cu-SAPO-34 reported here might not provide a strict like-for-like comparison, the identical framework structure of SSZ-13 and SAPO-34 allows for an assessment of the importance of specific  $\text{Cu}^{2+}$  sites on the activity for  $\text{NH}_3$ -SCR.

## 2. Experimental

### 2.1. Catalyst synthesis

#### 2.1.1. Synthesis of SSZ-13 parent material

SSZ-13 was prepared from an unseeded reaction mixture forming a gel with the following molar composition: 10 TMAda-OH: 5  $\text{Na}_2\text{O}$ : 4  $\text{Al}_2\text{O}_3$ : 100  $\text{SiO}_2$ : 2200  $\text{H}_2\text{O}$ . The gel was prepared by first mixing solutions of NaOH (1 M, VWR), TMAda-OH (N,N,N-trimethyl-1-adamantanionium hydroxide, 1 M, Sachem ZeoGen 2825) and deionized water.  $\text{Al}_2\text{O}_3$  (54% hydrate, Aldrich) was then added to the solution and stirred until the powder was dissolved. This mixture was mixed with Cab-O-Sil M5 (Cabot) fumed silica.

The resulting viscous gel was homogenized by hand for 5 min and aged at room temperature for 2 h. The gel was then heated statically for 4 days at 160 °C in a 15 mL Teflon lined steel autoclave.

#### 2.1.2. Conventional wet ion exchange

Cu-SSZ-13-WIE (CZ-WIE) was prepared via conventional wet ion exchange of the parent SSZ-13 (0.91 g) with a solution of 0.1 M  $\text{CuSO}_4$  (Merck) in 50 mL water. The slurry was continuously stirred for 3 h at 80 °C. The exchanged zeolite was separated using vacuum filtration, dried overnight at 120 °C and further calcined at 500 °C to obtain Cu-SSZ-13 [7]. The sample is henceforth referred to as CZ-WIE.

#### 2.1.3. Chemical vapor deposition ion exchange

Cu-SSZ-13-CVD (CZ-CVD) was prepared by first drying Cu-nitrate (5x stoichiometric excess) and SSZ-13 (separately) in an inert atmosphere at 120 °C for 1 h. The zeolite was then transferred into the same reactor as the metal salt. The materials were separated by a thin layer of glass wool. The system was heated to 250 °C in a He flow, with a ramp of 1 °C/min and a dwell time of 5 h. The resulting  $\text{HNO}_3$  was trapped in a water bath connected to the outlet of the reactor. The system was then cooled down and the zeolite 'layer' was collected and washed with distilled  $\text{H}_2\text{O}$ . The powder was left to dry at 120 °C overnight and further calcined at 550 °C with a heating ramp of 2 °C/min. The sample is henceforth referred to as CZ-CVD.

#### 2.1.4. Direct synthesis of Cu-SAPO-34

Silicoaluminophosphate gels were prepared by mixing  $\text{Al}(\text{OH})_3$  with  $\text{H}_3\text{PO}_4$  (85%) and fumed silica in water, followed by addition of the copper complex  $(\text{Cu}(\text{triethylenetetramine})^{2+})$  (CuTETA) and finally tetraethylammonium hydroxide (TEAOH) until a pH of 7 is achieved. Gels were typically of molar ratio Al: 0.8 P: 0.2 Si: 40  $\text{H}_2\text{O}$ : 0.030–0.125 CuTETA: x TEAOH. The Cu complex of triethylenetetramine was prepared initially by adding the polyamine to aqueous solutions of the metal acetate salt. A portion of the total water content was set aside for this purpose. The solution was then introduced to the gel. All gels were stirred continuously at room temperature during the preparation process until homogeneous, prior to being loaded in Teflon-lined stainless steel autoclaves and heated in the oven at 190 °C for seven days.

### 2.2. Catalyst characterization

#### 2.2.1. Synchrotron X-ray powder diffraction

Synchrotron X-ray powder diffraction on CZ-WIE was performed at the Swiss-Norwegian beamline (SNBL; BM01) in the European Synchrotron Research Facility (ESRF), Grenoble, France. The measurements were performed on powdered samples packed (sieve fractions of 90–125  $\mu\text{m}$ ) in 2 mm quartz capillaries. X-ray diffraction was recorded between 2–25° 2 $\theta$  at a wavelength ( $\lambda$ ) of 0.50117 Å using 5 scintillation detectors. The diffraction data was then summed and averaged over all the detectors. Rietveld refinement of X-ray diffraction data (2.8–20° 2 $\theta$ ) was performed using the FULLPROF [21] package along with the WinPLOTR interface [22]. The initial hexagonal unit cell dimensions ( $a = b = 13.675$  Å;  $c = 14.767$  Å) with a  $R\bar{3}m$  space group was taken from the International Zeolite Association (IZA) website for the CHA framework [23]. Starting atomic co-ordinates were taken from the suggested structure by Fickel et al. [7]. The background profile was edited manually by choosing 40 points over the pattern and further using a cubic-spline interpolation. The peak profiles were modeled using a Pseudo-Voigt function, whilst accounting for asymmetry below 10° 2 $\theta$ . Only symmetry constraints were used while modeling the position of atoms in the unit cell. All

tetrahedral positions were modeled as Si atoms. The displacement parameters ( $B_{\text{iso}}$ ) for all oxygen atoms were refined with the same value during the refinement

Synchrotron X-ray powder diffraction on Cu–SAPO-34 was performed at the Beamline I-11 on the Diamond Light Source Synchrotron [24]. A sample of Cu–SAPO-34 was calcined at 570 °C, loaded into a 0.5 mm quartz glass capillary, dehydrated, pre-treated in  $\text{O}_2$  at 250 °C for 2 h and finally evacuated at 120 °C at  $10^{-4}$  mbar before being sealed. The sample was then examined in Debye–Scherrer geometry using X-rays of wavelength 0.825028 Å. To minimize the effects of beam damage, eight data sets were collected for three minutes each over the range of  $1\text{--}140^\circ 2\theta$ , with a fresh portion of the sample exposed to the beam by translating the capillary between collections. The eight data sets were summed and binned on a  $0.002^\circ$  step size. Data at  $2\theta$  angles greater than  $30^\circ$  were discarded, as the intensity of the peaks strongly decreased. Finally, the data were re-binned to a step size of  $0.003^\circ$ . The diffraction pattern was collected at  $-173^\circ\text{C}$ . Rietveld refinement of the instrumental parameters and the Cu–SAPO-34 structure against the diffraction profiles was performed using the GSAS suite of programs using the SAPO-34 framework structure as a starting model for the calcined material [25]. The profile was modeled using a Pseudo-Voigt function and the background was modeled with a 36 term cosine function. The framework Al–O and (P, Si)–O distances were constrained during the refinement to 1.73(2) Å and 1.52(2) Å, respectively, and O–O distances were constrained to 2.82(5) Å (for  $\text{AlO}_4$  tetrahedra) and 2.49(5) Å for (P, Si) $\text{O}_4$  tetrahedra. Difference Fourier analysis and iterative refinement of positions and occupancies were used to locate extra-framework  $\text{Cu}^{2+}$  cations.

### 2.2.2. Synchrotron X-ray absorption

X-ray absorption experiments were performed on CZ–WIE and CZ–CVD at BM1, SNBL, under the same conditions as mentioned above. Using a Si(111) double crystal monochromator, X-ray absorption data at the Cu K-edge (8979 eV) was collected in transmission mode. Cu K-edge X-ray absorption on Cu–SAPO-34 was measured at the Dutch–Belgian beamline (BM26) using a Si(111) double crystal monochromator also in transmission mode [26]. The XAFS data were background corrected using the Athena package (IFEFFIT software package). The normalized data was  $k^3$ -weighted and the analysis performed in a  $k$ -range of  $2.8\text{--}10\text{ Å}^{-1}$ . The FT of the  $k^3$ -weighted data were phase corrected and fit to the proposed theoretical model using the DL-EXCURV program [27].

### 2.3. $\text{NH}_3$ –SCR activity tests

Catalytic tests were performed using an in-house built catalytic rig and under plug flow conditions using 200 mg of powdered catalyst (sieve fractions of 0.45–0.125 mm). A feed composition of 1000 ppm NO, 1000 ppm  $\text{NH}_3$  and 5%  $\text{O}_2$  (with He for balance) was used adding up to a Gas Hourly Space Velocity (GHSV) of  $100000\text{ h}^{-1}$ . All gases were provided by Linde and the flows were controlled using a set of Brooks 5850 mass flow controllers. To study their activity, Cu–CHA samples were heated from 50 to 500 °C at a rate of 5 °C/min, whilst the output gases were analyzed online by mass spectrometry (MS, Hiden Analytical, HPR-20 QIC), and infrared (IR) spectroscopy (Perkin–Elmer, Spectrum One). A gas cell with KBr windows and a path length of  $\sim 5\text{ cm}$  was used for the IR analysis. The spectra were measured in a continuous mode using the Perkin–Elmer ‘Time-Base’ software between  $4000\text{--}700\text{ cm}^{-1}$  wavenumbers with a spectral resolution of  $8\text{ cm}^{-1}$  and an acquisition of 40 scans per spectrum, resulting in a time interval of 44 s between each spectrum.

## 3. Results and discussion

### 3.1. Catalytic performance

All catalysts were tested under plug flow conditions for the SCR of NO using  $\text{NH}_3$  as the reducing agent. Fig. 1 compares the conversion of NO over the Cu–CHA catalysts as a function of temperature. As clearly seen, CZ–WIE and Cu–SAPO-34 are excellent catalysts for  $\text{NH}_3$ –SCR. Of particular interest is the high activity shown by these systems even at lower temperatures, i.e.  $<250^\circ\text{C}$ , which was not observed for metal exchanged zeolites studied in the past [2,3]. Whilst Cu–SAPO-34 and CZ–WIE both show remarkable activity over a very wide temperature range ( $>90\%$  conversion between  $\sim 175\text{--}375^\circ\text{C}$ ), CZ–CVD was found to show high activity only between  $\sim 225\text{--}350^\circ\text{C}$ . The low amount of copper present in this catalyst (Table 1) could account for the change in activity. However, a comparison of the activity profile of CZ–CVD to that of a Cu–SSZ-13 sample prepared via wet ion exchange, but with a similar Cu loading as CZ–CVD (Fig. S1) suggests it is the type of Cu species rather than Cu loading which causes the observed change.

Fig. 2 illustrates the selectivity of the Cu–CHA catalysts towards the desired  $\text{N}_2$  and undesired  $\text{N}_2\text{O}$  formation. Although the NO conversion profile appears identical for CZ–WIE and Cu–SAPO-34, the latter appears to be more selective to  $\text{N}_2$ , whilst small amount of  $\text{N}_2\text{O}$  ( $\sim 30\text{ ppm max}$ ) are seen to form over the former. CZ–CVD on the other hand, forms a much larger amount of undesired  $\text{N}_2\text{O}$  ( $\sim 250\text{ ppm}$  at  $275^\circ\text{C}$ ) as compared to the other two catalysts over the tested temperature range. The highest amount of  $\text{N}_2\text{O}$  formed is concurrent with the highest observed activity, suggesting competing  $\text{N}_2$  and  $\text{N}_2\text{O}$  formation over CZ–CVD.  $\text{N}_2\text{O}$  formation under SCR conditions can proceed via the following four possible reaction pathways, especially at low temperatures:

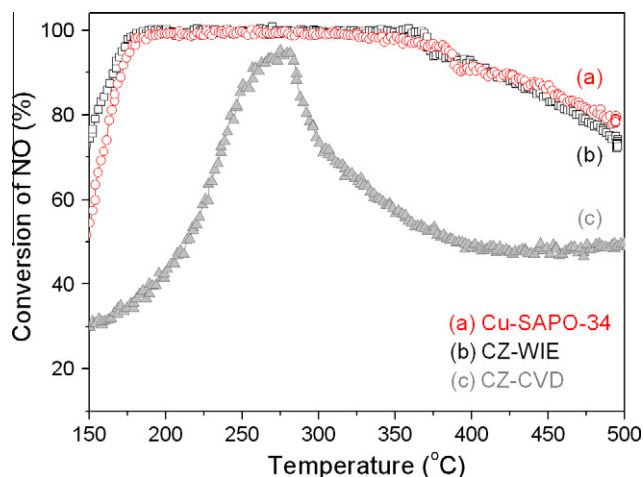


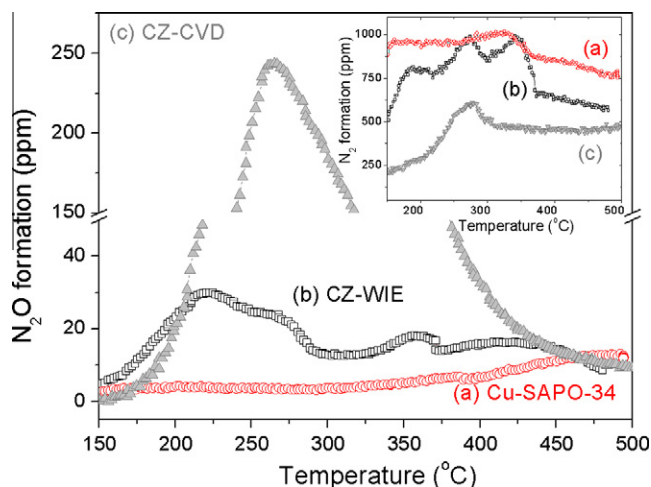
Fig. 1. Conversion of NO over (a) Cu–SAPO-34 (red); (b) CZ–WIE (black) and (c) CZ–CVD (grey). Plug flow conditions: 1000 ppm NO; 1000 ppm  $\text{NH}_3$ ; 5%  $\text{O}_2$ ; GHSV:  $100000\text{ h}^{-1}$ . (For interpretation of the references to colours in this figure legend, the reader is referred to the web version of this paper.)

Table 1

Copper loading (wt.%) for Cu–CHA catalysts used in this study.

Sample	Cu wt.% <sup>a</sup>
Cu–SAPO-34	4.91
CZ–WIE	3.60
CZ–CVD	1.83

<sup>a</sup> Obtained from ICP analysis.



**Fig. 2.** Formation of  $\text{N}_2\text{O}$  as a by-product during  $\text{NH}_3$ -SCR for (a) Cu-SAPO-34 (red); (b) CZ-WIE (black) and (c) CZ-CVD (grey). Inset: Formation of  $\text{N}_2$  during the same reaction. Plug flow conditions: 1000 ppm NO; 1000 ppm  $\text{NH}_3$ ; 5%  $\text{O}_2$ ; GHSV:  $100000\text{ h}^{-1}$ . (For interpretation of the references to colours in this figure legend, the reader is referred to the web version of this paper.)

- (a)  $3\text{NO} \rightarrow \text{N}_2\text{O} + \text{NO}_2$ ;
- (b)  $2\text{NH}_3 + \text{O}_2 \rightarrow \text{N}_2\text{O} + 3\text{H}_2\text{O}$ ;
- (c)  $4\text{NO} + 4\text{NH}_3 + 3\text{O}_2 \rightarrow 4\text{N}_2\text{O} + 6\text{H}_2\text{O}$ ;
- (d)  $4\text{NO}_2 + 4\text{NH}_3 + \text{O}_2 \rightarrow 4\text{N}_2\text{O} + 6\text{H}_2\text{O}$ ;

It is known that in the absence of metal species,  $\text{NH}_3$ -SCR over a parent zeolite (e.g. H-ZSM-5) leads to both a drop in activity and an increase in the formation of  $\text{N}_2\text{O}$  [18,28]. However, in the case of a parent zeolite, the activity profile (hence concurrent  $\text{N}_2\text{O}$  formation) is shifted to higher temperatures ( $\sim 300^\circ\text{C}$  for SSZ-13;  $350^\circ\text{C}$  for ZSM-5), which is not the case for CZ-CVD. Therefore the contribution of the CHA framework towards  $\text{N}_2\text{O}$  formation can be ruled out. High temperature  $\text{N}_2\text{O}$  formation ( $>350^\circ\text{C}$ ) has been attributed to the side reaction of ammonia oxidation, especially over Cu-based catalysts [29]. It is possible that the slight amounts (max. 15–20 ppm) of  $\text{N}_2\text{O}$  formation seen at higher temperatures for CZ-WIE and Cu-SAPO-34 is due to ammonia oxidation. However, for CZ-CVD very little  $\text{N}_2\text{O}$  is seen at temperatures above  $350^\circ\text{C}$ . In fact, the outlet composition above  $300^\circ\text{C}$  (Fig. 2 and inset) shows a steady formation of  $\text{N}_2$  although there is a clear drop in the NO conversion profile. This indicates that the available  $\text{NH}_3$  from the feed is converted to  $\text{N}_2$  rather than to  $\text{N}_2\text{O}$ .

$\text{N}_2\text{O}$  formation over Cu systems under SCR conditions has been previously observed and been mainly attributed to the presence of CuO aggregates or Cu dimers  $[\text{CuOCu}]^{2+}$  formed over  $\text{Al}_2\text{O}_3$ ,  $\text{TiO}_2$  or zeolite (e.g. FAU, OFF) supports [30–34]. Studies performed on  $\text{N}_2\text{O}$  decomposition reactions on the other hand propose Cu dimers such as  $[\text{CuOCu}]^{2+}$  to be active intermediates being formed during the decomposition reaction [35].

### 3.2. Local Cu environment(s) in the Cu-CHA catalysts

#### 3.2.1. Cu-SAPO-34

Cu-SAPO-34 prepared via a direct synthetic route enabled us to obtain a Cu-CHA catalyst by avoiding the process of aqueous ion-exchange during which the zeolite structure is prone to suffer hydrolytic damage. Diffuse reflectance UV-vis-NIR spectra of Cu-SAPO-34 (after calcination) indicate the presence of  $\text{Cu}^{2+}$  species ( $\text{Cu}^{2+}$  d-d transition  $\sim 12000\text{ cm}^{-1}$  and LMCT ( $\text{O} \rightarrow \text{Cu}$ )  $\sim 40000$  and  $\sim 47000\text{ cm}^{-1}$ ; Fig. S2(a)). No evidence for other Cu species such  $\text{Cu}^+$  or binuclear Cu-O-Cu type species was found [36].

Laboratory based powder XRD (Fig. S3) shows retention of the SAPO-34 structure after calcination. Fig. S4 shows the solid-state NMR spectra collected on the sample.  $^{29}\text{Si}$  MAS NMR (Fig. S4, left) indicates that most of the  $\text{Si}^{4+}$  present replaces  $\text{P}^{5+}$  in the aluminophosphate framework, although there is an indication for the presence of Si-rich domains as seen from the shoulders around  $-105$  to  $-112\text{ ppm}$  [37,38].  $^{27}\text{Al}$  MAS NMR (Fig. S4, right) indicates all  $\text{Al}^{3+}$  in the as-prepared samples is tetrahedrally-coordinated, ruling out the presence of extra-framework  $\text{Al}^{3+}$ .

Synchrotron X-ray powder diffraction was performed on calcined Cu-SAPO-34 with the aim of determining the  $\text{Cu}^{2+}$  location, but the refinement was made difficult by disorder of the framework structure. The Cu-SAPO-34 sample has an intergrown morphology (Fig. S5) and the diffraction pattern possesses broad reflections at d-spacings of 6.74, 5.16 and  $4.2\text{ \AA}$  (Fig. S6) that indicate structural disorder. Comparison with the diffraction patterns predicted by Lillerud et al. [39] for series of CHA structures with different levels of intergrowing polytypic AEI structure suggest that this kind of disorder may be responsible for the broad reflections. The CHA/AEI intergrowth is possible because the structures share a common plane of  $d6r$  rings: in CHA all  $d6r$ s have the same orientation whereas in AEI adjacent planes of  $d6r$ s have alternating orientations. Due to this intergrowth, attempts at refinement were not successful. However, a second Cu-SAPO-34 sample (Cu-SAPO-34B, unit cell composition of as-prepared form  $(\text{CuL})_{0.8}(\text{NC}_8\text{H}_{20})_{2.2}\text{Si}_{4.5}\text{P}_{13.5}\text{Al}_{18}\text{O}_{72}$ ) with about half the copper content of the sample tested for catalysis was synthesized using the same experimental approach. This sample appeared to have a lower level of intergrowth and could be analyzed using Rietveld refinement of synchrotron X-ray powder diffraction data collected on a calcined sample. Fig. 3 shows the observed, calculated and difference profiles for Cu-SAPO-34B after calcination and dehydration as obtained from Rietveld refinement of powder diffraction data, along with the obtained crystal structure (inset). Sites for  $\text{Cu}^{2+}$  cations were located via difference Fourier analysis above the six-member ( $6m$ ) rings of the  $d6r$  sub-units of the CHA structure (Fig. 3, inset). Note that the (inset) figure illustrates 3 symmetrically equivalent copper atoms (sites), with a fractional occupancy of 0.069. Based on this, at most, only one  $\text{Cu}^{2+}$  will be present for every  $d6r$  unit at any given time. Additional scattering was refined as  $\text{Cu}^{2+}$  at a second site close to  $4mrs$  of the structure but this gave unreasonably short Cu-P and Cu-O distances. Hence, for the sake of chemical clarity, we disregard the presence of copper at this site, although the presence of a second site is required by the discrepancy between the  $\text{Cu}^{2+}$  known by analysis to be present and the amount located at the  $d6r$  site. The refinement parameters are presented in Table 2 and the relevant bond distances and angles are presented in Table 3.

XANES data were collected on Cu-SAPO-34 (Fig. 4) to follow the decomposition of the copper-triethylenetetramine SDA during calcination. The two most interesting features are marked as 1 and 2 and vary as a function of temperature. The spectrum measured at  $100^\circ\text{C}$  shows two clear contributions around the absorption edge (marked 1) which has been seen previously for Cu in a square planar 'amine' environment [40–42]. Chaboy et al. were able to explain this contribution by using two final state configurations of  $3d^9$  and  $d^{10}\text{L}$  ( $\text{L}$  = ligand hole) for the absorber atom. During the process of calcination, the ligand gets 'burnt' off resulting in the gradual disappearance of this feature as a function of temperature. Feature 2 at the absorption threshold follows the opposite trend, i.e. it starts to appear during the process of calcination and is distinctly visible in the final sample. This has been observed in the past in  $\text{Cu}^{2+}$ -exchanged zeolites and can be assigned to a  $\text{Cu}^{2+} 1s \rightarrow 4p_z$  + ligand- $\text{Cu}^{2+}$  charge transfer (CT) excitation very similar to that seen in  $\text{Cu}(\text{OH})_2$  with the Cu in a planar geometry [36]. These changes are indicative of the template-removal process

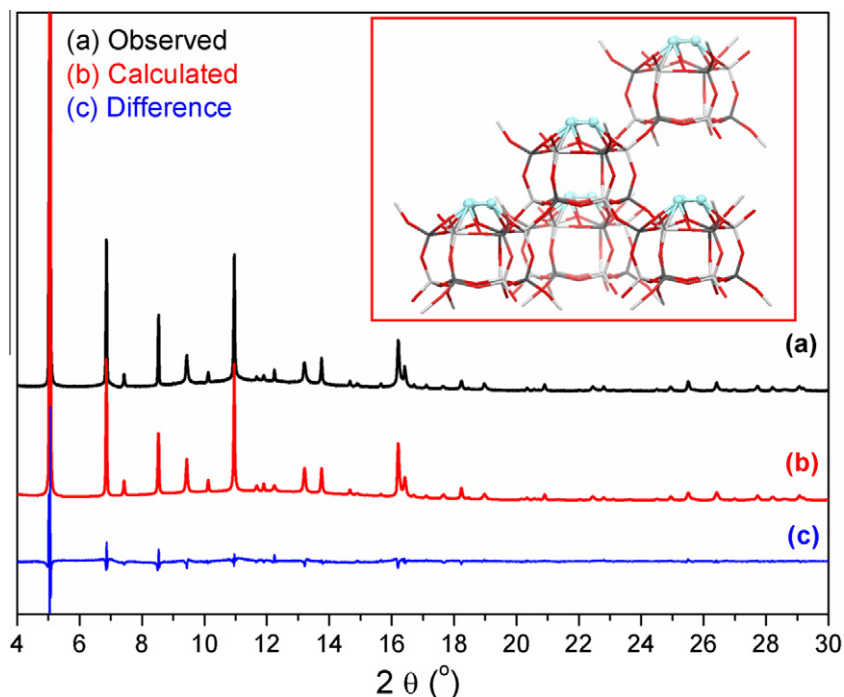


**Fig. 3.** Rietveld refinement of synchrotron X-ray powder diffraction data collected on Cu-SAPO-34B after calcination. Key: Observed data (black), calculated fit (red) and relative difference curve (blue). Inset: Crystal structure of Cu-SAPO-34B as obtained from the refinement. NOTE: Copper atoms are represented as blue balls and symmetrically equivalent sites with an occupancy of 0.06 per site. Therefore, only one (or less)  $\text{Cu}^{2+}$  is expected per d6r in the crystal structure. (For interpretation of the references to colours in this figure legend, the reader is referred to the web version of this paper.)

**Table 2**

Experimental parameters and goodness of fit factors obtained from Rietveld refinement of powder XRD data collected on calcined Cu-SAPO-34.

Experimental parameter	Value	Parameter	Value
Wavelength ( $\lambda$ )	0.8250 Å	$R_{wp}$	6.91
Scanned region ( $2\theta$ )	4–30	$R_p$	5.8
Refinement region ( $2\theta$ )	4–30	$R_{exp}$	0.74

**Table 3**

Calculated bond lengths and angles obtained from Rietveld refinement of powder XRD data collected on calcined Cu-SAPO-34.

Bond	Distance (Å)	Angle	Degrees
Si1/P1–O (Avg.)	1.567	O–Si1/P1–O (Avg.)	109.5
Si2/P2–O (Avg.)	1.567	O–Si2/P2–O (Avg.)	109.5
Al1–O (Avg.)	1.712	O–Al1–O (Avg.)	109.5
Al2–O (Avg.)	1.707	O–Al2–O (Avg.)	109.4
<b>T–O (Avg.)</b>	<b>1.638</b>	<b>O–T–O (Avg.)</b>	<b>109.47</b>
Cu–O6	2.44		
Cu–O7	2.78		

and subsequent movement of the  $\text{Cu}^{2+}$  cations to adopt coordination by framework oxidation.

### 3.2.2. CZ–WIE

Diffuse reflectance UV–vis–NIR measurements performed on CZ–WIE indicate the presence of  $\text{Cu}^{2+}$  species (d–d transition  $\sim 12000 \text{ cm}^{-1}$  and LMCT ( $\text{O} \rightarrow \text{Cu}$ )  $\sim 47000 \text{ cm}^{-1}$ ; Fig. S2(b)) similar to those prepared upon calcination of Cu-SAPO-34. The shift in the LMCT band compared to Cu-SAPO-34 gives an indication of a slightly different coordination of the Cu to the zeolite framework oxygens. Laboratory based powder XRD (Fig. S3(b)) showed no obvious visible damage to the crystal structure of the zeolite or agglomeration of Cu species as a result of the wet ion exchange.

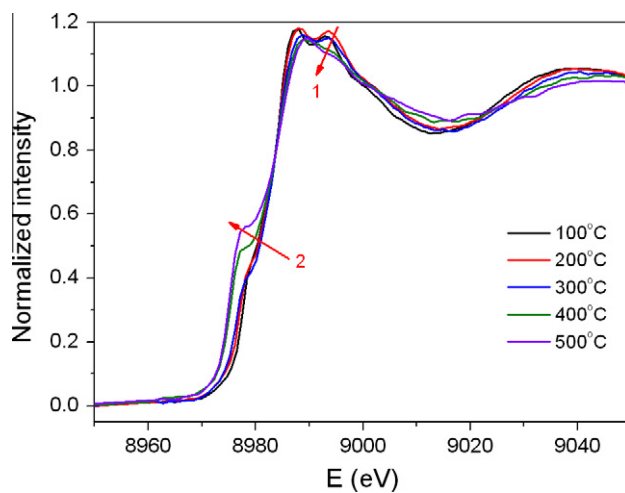


**Fig. 4.** Cu K-edge XANES spectra (normalized) of Cu-SAPO-34 during calcination measured at different temperatures. Features of interest are marked with numbered red arrows. (For interpretation of the references to colours in this figure legend, the reader is referred to the web version of this paper.)

Fig. S7 shows  $^{27}\text{Al}$  MAS NMR spectra of CZ–WIE compared to the parent (SSZ-13) zeolite. The spectrum of the calcined parent zeolite (Fig. S7(a)) consists of a relatively narrow resonance at 58 ppm, attributed to tetrahedrally-coordinated  $\text{Al}^{3+}$  in the zeolitic framework, which becomes broader after  $\text{Cu}^{2+}$ -exchange (Fig. S7(b)). No resonances typical of extra-framework octahedral  $\text{Al}^{3+}$  (c.a. 0 ppm) were observed indicating that no dealumination of the framework took place during the ion exchange.

Fig. 5 shows the observed, calculated and difference curve for CZ–WIE after calcination as obtained from Rietveld refinement of powder diffraction data along with the obtained crystal structure of CZ–WIE (inset). Experimental parameters and conventional

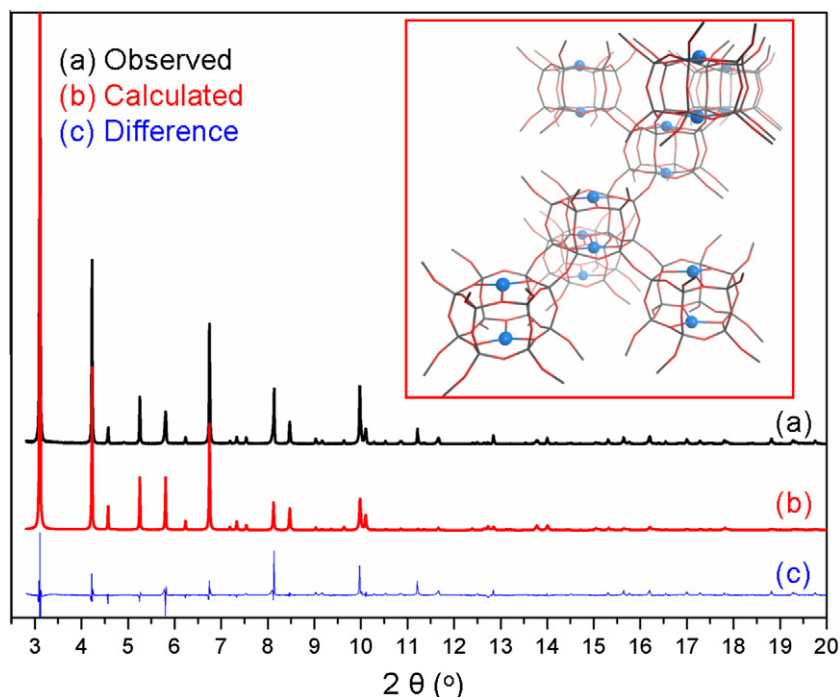


**Fig. 5.** Rietveld refinement of synchrotron X-ray powder diffraction data collected on CZ-WIE after calcination. Key: Observed data (black), calculated fit (red) and relative difference curve (blue). Inset: Crystal structure of CZ-WIE as obtained from the refinement. NOTE: Copper atoms are represented by blue balls at (symmetrically equivalent) mirror image sites on either face of the *d6r*. (For interpretation of the references to colours in this figure legend, the reader is referred to the web version of this paper.)

**Table 4**

Experimental parameters and goodness of fit factors obtained from Rietveld refinement of powder XRD data collected on calcined CZ-WIE.

Experimental parameter	Value	Parameter	Value
Wavelength ( $\lambda$ )	0.50117 Å	$R_{wp}$	24.9 (18.2)
Scanned region ( $2\theta$ )	2–25	$R_p$	19.1 (13.4)
Refinement region ( $2\theta$ )	2.8–20	$R_{exp}$	12.98

**Table 5**

Calculated bond lengths and angles obtained from Rietveld refinement of powder XRD data collected on calcined CZ-WIE.

Bond	Distance (Å)	Angle	Degrees
T1–O1	1.61	O1–T–O2	107.7
T1–O2	1.62	O1–T–O3	110.2
T1–O3	1.61	O1–T–O4	113.5
T1–O4	1.58	O2–T–O3	106.0
<b>T1–O (Avg.)</b>	<b>1.60</b>	O2–T–O4	107.9
		O3–T–O4	111.0
<b>Cu–O1</b>	<b>2.32</b>	<b>O–T–O (Avg.)</b>	<b>109.38</b>
		T–O1–T	146.0
		T–O2–T	148.8
		T–O3–T	147.3
		T–O4–T	142.4
		<b>T–O–T (Avg.)</b>	<b>147.4</b>

goodness of fit parameters for the refinements along with the refined bond distances and angles obtained for Cu–CHA after calcination are listed in Tables 4 and 5 respectively. Cu was found to be present in the center of the six-member ring (*6mr*) plane (part of *d6r* sub-units) of the CHA structure. The obtained nearest Cu–O1 distance of 2.32 Å is in close agreement with previously reported values in literature on Cu exchanged SSZ-13 materials [7].

Fig. 6(a) illustrates the XANES spectra collected on CZ-WIE. Pre-edge features of interest are marked with numbers. Feature 1 highlights a pre-edge feature at ~8977 eV and has been magnified

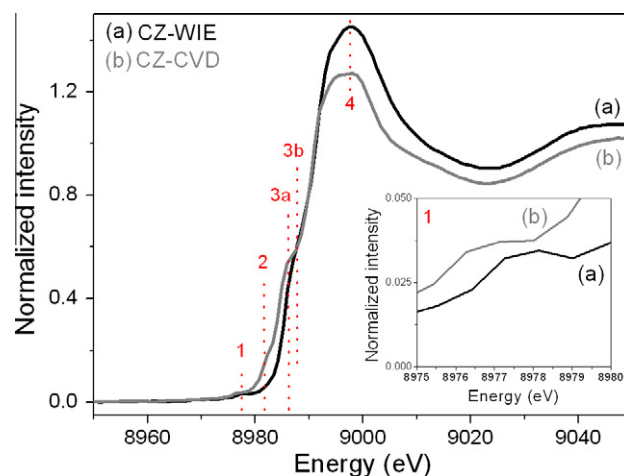


**Fig. 6.** Cu K-edge XANES spectra (normalized) of (a) CZ-WIE and (b) CZ-CVD. Features of interest are marked with numbered lines. Inset: Magnification of pre-edge feature (labeled 1) at ~8977 eV.

**Table 6**

Parameters obtained from MS analysis of Cu K-edge  $k^2$ -weighted EXAFS data collected on CZ-WIE after calcination.

Shells	$R$ (Å)	$N$	$2\sigma^2(\text{Å}^2)$
Cu–O	1.95	3	0.007
Cu–Si	2.20	2	0.037
Cu–O	2.93	1	0.008
Cu–O	3.32	2	0.016
Cu–Si	3.10	2	0.036
Cu–O	3.32	2	0.016
Cu–O	3.68	2	0.025
Cu–Cu	3.76	1	0.017
Cu–Si	4.08	2	0.032
Cu–Si	4.16	2	0.036
Cu–O	4.22	1	0.040
$R = 12.91\%$ ; $E_f = 1.28$			

(Fig. 6, inset) for clarity. This low intensity pre-edge has been assigned to a dipole forbidden  $1s \rightarrow 3d$  transition seen only in  $\text{Cu}^{2+}$  complexes [36,40,43,44]. The next feature of interest (marked 3b) appears at the absorption threshold ( $\sim 8986$  eV) and can be assigned to a  $\text{Cu}^{2+} 1s \rightarrow 4p_z$  + ligand- $\text{Cu}^{2+}$  charge transfer (CT) [36]. The absence of other pre-edge features below 8985 eV (apart from the pre-edge at 8977.27 eV) in CZ-WIE is a good indication for the presence of only  $\text{Cu}^{2+}$  in this system. The Cu K-edge  $k^3$ -weighted EXAFS data and corresponding Fourier transforms (FT) of CZ-WIE collected after calcination are illustrated in Fig. S8. The bond distances and coordination numbers thus obtained from multiple scattering (MS) calculations of the EXAFS data are presented in Table 6. The data reveals a slight distortion of the planar  $\text{Cu}^{2+}$  coordination environment, off-center in the  $6mr$  ring.  $\text{Cu}^{2+}$  is found to be closely coordinated to three framework oxygen atoms at a distance of 1.95 Å with an extra (fourth) oxygen at ca. 3.0 Å, in agreement with our previously-reported model [5]. Very recent single-crystal studies performed on  $\text{Cu}^{2+}$ -exchanged zeolite Y (FAU) show a 4-coordinate planar environment for  $\text{Cu}^{2+}$  in the  $6mr$  rings of the zeolite [45]. Similarly to our model, the authors claim three close oxygen atoms at distances between  $\sim 1.84$  and 1.95 Å for the two studied crystals, but in their studies the fourth oxygen was found at a distance of 2.20–2.32 Å in the highly distorted  $6mr$  ring. A possible explanation for this however could be the high aluminum content in their reported zeolite Y ( $\text{Si}/\text{Al} = 1.56$ ) as compared to the SSZ-13 reported herein ( $\text{Si}/\text{Al} = 18$ ). There is also an obvious difference in the Cu–O distance as obtained from the XRD analysis (2.32 Å) and that obtained from the EXAFS analysis (1.95 Å). The difference arises due to the fact that XAFS is a short range probing technique and hence is sensitive to small deviations within local structure, whilst diffraction being a long range order technique can only account for changes in the long range order of the material, and is further discussed by us elsewhere [9].

### 3.2.3. CZ-CVD

Chemical vapor deposition ion exchange was adapted to create isolated Cu species within a zeolite framework. Diffuse reflectance UV-vis-NIR measurements performed on CZ-CVD suggested the presence of only  $\text{Cu}^{2+}$  species (d–d transition  $\sim 12000$   $\text{cm}^{-1}$  and LMCT ( $\text{O} \rightarrow \text{Cu}$ )  $\sim 47000$   $\text{cm}^{-1}$ ; Fig. S2(c)). The intensity of the  $\text{Cu}^{2+}$  d–d transition band in the spectrum clearly suggests a lower  $\text{Cu}^{2+}$  concentration in CZ-CVD as compared to the other catalysts. Both  $^{27}\text{Al}$  MAS NMR (Fig. S7(c)) and laboratory based powder XRD (Fig. S3(c)) showed no structural damage/secondary species to the zeolite or visible agglomeration of Cu species as a result of the preparation method.

The very low amount of Cu present in the sample makes it challenging, in this case, to account for a reliable crystallographic position of Cu using diffraction. However, XAFS measurements can provide valuable insight into local Cu environment within the material. Fig. 6 (b) illustrates the XANES spectra of the sample after calcination. Pre-edge feature 1, present in CZ-CVD, is assigned to the dipole forbidden  $1s \rightarrow 3d$  transition seen in  $\text{Cu}^{2+}$  complexes [36,40,43,44] as discussed earlier. Pre-edge feature 2 between 8981–8983 eV appears to have a broadening effect on the absorption threshold of the spectrum. Finally pre-edge feature (3a) is seen closer to the absorption threshold at 8985.9 eV. Pre-edge features in this region have been previously assigned to a  $1s \rightarrow 4p$  transition most commonly seen in  $\text{Cu}^+$  systems. Linear  $\text{Cu}^+$  systems such as  $\text{Cu}_2\text{O}$  or  $\text{CuAlO}_2$ , are known to have an intense peak at  $\sim 8982$  eV owing to a transition from a  $1s$  orbital to a double degenerate  $4p_{xy}$  orbital [46]. On the contrary, in a 4-coordinate tetrahedral geometry, all  $p$  orbitals are closer to degeneracy, with a slight increase in their energy as compared to a doubly degenerate  $p_{xy}$  orbital. Hence,  $\text{Cu}^+$  complexes with a tetrahedral geometry are found to have a  $1s \rightarrow 4p_{xyz}$  transition at slightly higher energies of  $\sim 8585$  eV

**Table 7**

(Left) Parameters obtained from SS analysis of Cu K-edge  $k^3$ -weighted EXAFS data collected on CZ-CVD after calcination. (Right) Values obtained from literature for the local environment in  $\text{CuAlO}_2$ .

CZ-CVD				$\text{CuAlO}_2^a$		
Shells	$R$ (Å)	N	$2\sigma^2(\text{\AA}^2)$	Shells	$R$ (Å)	N
Cu–O	1.95	3.1	0.012	Cu–O	1.86	2
Cu–Cu	2.92	2.4	0.032	Cu–Cu	2.87	6
Cu–Cu	3.38	3	0.010	Cu–Al	3.28	6
Cu–Al	3.39	2.9	0.023	Cu–O	3.42	12
$R = 14.15\%$ ; $E_f = -4.56$						

<sup>a</sup> Taken from literature (Ref. 39).

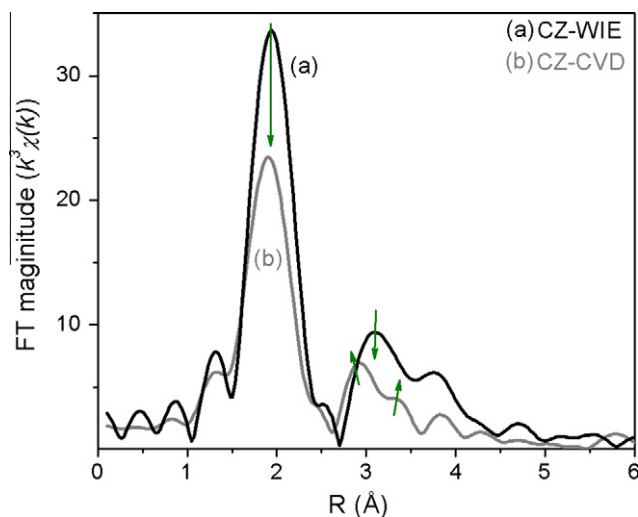


**Fig. 7.** Fourier transforms of  $k^3\chi(k)$  EXAFS data collected for (a) CZ-WIE and (b) CZ-CVD after calcination at RT. Green arrows point to differences seen in both spectra. (For interpretation of the references to colours in this figure legend, the reader is referred to the web version of this paper.)

as is seen in CZ-CVD (marked 3a) [43]. However,  $\text{Cu}^{2+}$  in a tetragonal geometry (such as in  $\text{CuO}$ ) is also known to have a  $1s \rightarrow 4p_z$  transition reflected by a pre-edge shoulder at  $\sim 8985$  eV. Although feature 3a cannot be conclusively assigned as either  $\text{Cu}^{2+}$  or  $\text{Cu}^+$ , the presence of all three features (marked 1, 2 and 3a) in CZ-CVD is an indication for the presence of more than one Cu environment, most likely with more than one oxidation state. Finally, it is worth to note feature 4 which highlights a drop in the rising absorption edge intensity and hence the difference in the number unoccupied electronic states of the absorber atom in each catalyst.

Using the same model as proposed for CZ-WIE, EXAFS data collected on CZ-CVD was analyzed using single scattering paths. The  $k^3$ -weighted EXAFS experimental data and corresponding FTs are shown in Fig. S8(c and d) along with the simulated fits. The obtained coordination and bond distances are listed in Table 7 whilst Fig. 7 contains a comparison of the EXAFS FTs for both CZ-WIE and CZ-CVD. A drop in the intensity of the first peak at  $\sim 1.9$  Å and changing features at  $\sim 2.8$ – $2.9$  Å indicate a clear change in the Cu–O interactions in CZ-CVD. Furthermore, the change in the width of the first peak at  $\sim 2.1$  Å and the missing contribution at  $\sim 3.1$  Å for CZ-CVD suggest a different (or missing) Cu–Si interaction. We also observe two new contributions at  $\sim 2.9$  Å as a result of a Cu–Cu contribution and at  $\sim 3.4$  Å due to a Cu–Al contribution.

Recent Cu K-edge XAFS studies performed on  $\text{CuAlO}_2$  suggest the presence of two nearest neighbor oxygens at a distance of 1.86 Å, followed by six Cu at 2.87 Å and six aluminums at 3.28 Å, in agreement with previous single crystal diffraction studies per-

**Table 8**

Structure-performance co-relations between the three Cu-CHA catalysts prepared via different methods.

Sample name	Local Cu environment	deNO <sub>x</sub> activity	deNO <sub>x</sub> selectivity <sup>a</sup>
Cu-SAPO-34	Isolated Cu <sup>2+</sup> slightly above the plane of <i>d6r</i> sub-unit	V. High (~175–350 °C) <sup>b</sup>	High
CZ-WIE	Isolated Cu <sup>2+</sup> in the plane of <i>d6r</i> ring sub-units	V. High (~175–350 °C) <sup>b</sup>	High
CZ-CVD	Isolated Cu <sup>2+</sup> and Cu-aluminate type species	Very low (~250–300 °C) <sup>b</sup>	Very low, N <sub>2</sub> O formation

<sup>a</sup> deNO<sub>x</sub> selectivity towards the formation of desired N<sub>2</sub> is a final product.

<sup>b</sup> Temperature window of >90% activity.

formed on the same [46]. The CuAlO<sub>2</sub> environment thus obtained is listed in Table 7 for comparison. The structure of CuAlO<sub>2</sub> is composed of alternating layers of linear Cu (coordinated to two oxygens) and Al-O<sub>6</sub> octahedra. Given the correlation between the bond distances obtained by us and those mentioned in literature, we propose the presence of CuAlO<sub>2</sub> type species in CZ-CVD alongside isolated Cu<sup>2+</sup> ions. Since we have more than one type of Cu species present in this material, any analysis obtained from the EXAFS data would only provide us with a linear combination of the different Cu local environments in question. Hence there is a small difference in coordination number/bond distance obtained for the CZ-CVD sample when compared to pure CuAlO<sub>2</sub>.

### 3.3. Relation of local Cu structure with performance in Cu-CHA catalysts

As is evident, the nature of Cu sites within the CHA framework can differ as a function of the preparation technique, which in turn has a direct influence on the catalytic performance of the catalyst. Table 8 relates the local Cu environment in each catalyst to the catalytic performance of each catalyst.

A general observation from the structure of the support was the tendency of Cu to have a preference towards the *d6r* sub-units of the CHA structure. Since CZ-WIE has a unique position for isolated Cu<sup>2+</sup>, this provides us with a good basis for active site comparison with the other catalysts. A very recent study performed on Cu-SSZ-13 and Cu-SAPO-34 reported 15% and 45% respectively of Cu<sup>+</sup> present in the catalysts under operando SCR conditions at 200 °C [47]. We do not see any indication towards the presence of Cu<sup>+</sup> in either CZ-WIE or Cu-SAPO-34 used in this study, or under in situ SCR conditions in Cu-SSZ-13 (analogous to CZ-WIE) [9]. Studies performed in the past have compared and shown a similar activity of Cu-SSZ-13 and Cu-SAPO-34 [18,48]. However the studies used ion-exchanged Cu-SAPO-34 and hence were limited by the amount of copper they could introduce into the specific extra-framework positions. In the Cu-SAPO-34 presented herein, we could control the amount of Cu<sup>2+</sup> introduced into the framework. Considering the identical activity profiles of Cu-SAPO-34 and CZ-WIE, the presence of additional Cu (and at more than one site) does not seem to have an apparent advantage to the deNO<sub>x</sub> activity. To test this hypothesis further, activity tests were performed at much higher Gas Hourly Space Velocity (GHSV) of 600000 h<sup>-1</sup> (6 times higher than previously discussed). The tests reveal that at extreme space velocities, the support material starts to play a major role as illustrated in Fig. S9. Whilst there is little change in the activity profile of CZ-WIE (as compared to the activity at a GHSV of 100000 h<sup>-1</sup>), Cu-SAPO-34 appears to have a slight drop in the NO conversion profile with a maximum of 80% conversion at ~300–350 °C.

Cu-SAPO-34 exhibits a higher selectivity towards N<sub>2</sub> compared to CZ-WIE (Fig. 2). Consequently, at lower temperatures, N<sub>2</sub>O formation is completely avoided over Cu-SAPO-34, whilst CZ-WIE forms slight amounts (<30 ppm). Although none of the characterization techniques show a secondary Cu phase present in CZ-WIE, one cannot completely rule out the presence of very small amounts of impurities in the sample. This could be a possible explanation for the N<sub>2</sub>O formed at lower temperatures. Secondly, considering the higher Cu-loading in Cu-SAPO-34, a higher occupancy at the active sites (*6mr* rings) might be expected. It is known that NO can form NO<sub>2</sub> in the presence of oxygen. At temperatures below 250 °C, NO<sub>2</sub> was found in the outlet gases for CZ-WIE (not shown) but not for Cu-SAPO-34. Compared with CZ-WIE, the availability of additional (or more) Cu<sup>2+</sup> in *6m* ring site, especially at the lower temperatures, appears to consume the NO<sub>2</sub> formed over Cu-SAPO-34 leading to a higher amount of N<sub>2</sub> formed. At temperatures above 350 °C, whilst the NO conversion drops, N<sub>2</sub> and small amounts of N<sub>2</sub>O (<17 ppm) form over Cu-SAPO-34. This is attributed to the high activity for NH<sub>3</sub> oxidation exhibited by this catalyst, as has also been seen in the past over Cu-exchanged zeolites [49,50]. The higher amount of Cu present in Cu-SAPO-34 (considering multiple sites) helps avoid ammonia slip at these temperatures. However, as seen from the NO conversion activity, and the tests performed at extreme GHSV, additional copper (also at other possible cationic positions) does not seem to have an influence in the SCR reaction.

Comparing the XAFS data for CZ-WIE and CZ-CVD led us to conclude that in the latter, a secondary phase of CuAlO<sub>2</sub> is present. This results in a diminished activity and selectivity for N<sub>2</sub> production but enhanced activity for N<sub>2</sub>O production. The CVD-IE process is driven by the formation of gaseous HNO<sub>3</sub> as a by-product upon the decomposition of Cu(NO<sub>3</sub>)<sub>2</sub> and subsequent exchange of Cu ions with charge compensating H<sup>+</sup> ions in the zeolite. It has also been observed in the past in attempts to load zeolite Y with InCl, that removal of the anionic species is both slow and can be incomplete [51]. This enhances the chances of interaction of the slowly forming acids with the zeolite framework, which appears then to lead to a partial dealumination of the zeolite and formation of small CuAlO<sub>2</sub> crystallites. Neither CuO aggregates nor Cu-dimers previously proposed to be responsible for N<sub>2</sub>O formation under SCR conditions in Cu-zeolite were observed in our system [30–34].

## 4. Conclusions

Cu-CHA catalysts were prepared via three different synthetic approaches and tested in the reduction of NO using NH<sub>3</sub> as a reducing agent. Each approach leads to the formation of different local environments for Cu within the zeolite pores, and the different species formed are not equally effective for the SCR reaction.

The location of isolated Cu<sup>2+</sup> ions on or close to the plane of the six-member ring in CZ-WIE and Cu-SAPO-34 appears crucial for the excellent activity and selectivity demonstrated by these two catalysts. These are the active sites for the NH<sub>3</sub>-SCR reaction as seen by the direct correlation between activity/selectivity and presence of Cu<sup>2+</sup> at this site. Copper present at additional sites (as in the case for Cu-SAPO-34) does not seem to benefit the SCR reaction. Furthermore, it appears that the support material starts to play a role as we move to extreme Gas Hourly Space Velocities. While little change is observed in the conversion of NO over the zeolite based catalyst, Cu-SAPO-34 appears to demonstrate a slightly lower activity at these extreme flows. The vapor deposition approach led to the formation of, besides isolated Cu<sup>2+</sup>, a dominant secondary phase similar in structure to CuAlO<sub>2</sub>. This results in a poor deNO<sub>x</sub> activity and a high selectivity towards the formation of undesired N<sub>2</sub>O.

The study enables comparison of the different preparation methods. Vapor deposition, although intended to create isolated metal ions, is not suitable in this particular case. The process itself is driven by the formation of an acid, which appears to facilitate partial dealumination and subsequent formation of unwanted copper aluminate species. The technique also demands a vacuum or inert atmosphere to successfully sublime the metal salts and initiate the exchange process. The one-pot synthetic approach, besides its inherent benefit of being a one-step process, permits control of cation content by modifying the synthetic procedure, and homogeneous distribution of copper cations upon calcination of the template (no long range cation diffusion processes are required). The approach is, however, restricted to those zeolitic systems that can be prepared with coordination complexes as templates, which remains limited. Conventional wet ion exchange is, at least for the aluminosilicate material in this particular case, easy to perform, cost-effective and results in active catalysts with copper present in the desired cationic locations.

### Acknowledgements

This research was carried out under project number M23.7.08301 in the framework of the Research Program of the Materials innovation institute M2i ([www.m2i.nl](http://www.m2i.nl)). Einar A. Eilertsen (University of Oslo) is thanked for the synthesis of the SSZ-13 parent material. The authors would like to thank Sachem inc. for kindly providing the template (ZeoGen 2825) used in the synthesis of SSZ-13. Inés Dácil González-Jiménez (Utrecht University) is thanked for helping with experiments at SNBL, ESRF. ESRF is thanked for providing access to combined in situ XAFS/XRD facilities. We thank Dr. Stephen Thompson and Professor Chiu C. Tang for assistance at the I11 beamline at the Diamond Light Source (DLS) and DLS for beamtime and Mr. Daniel Dawson and Dr. Sharon Ashbrook for collections of the solid-state NMR.

### Appendix A. Supplementary data

Supplementary data associated with this article can be found, in the online version, at <http://dx.doi.org/10.1016/j.micromeso.2012.04.056>.

### References

- [1] M. Iwamoto, H. Yahiro, K. Tanda, N. Mizuno, Y. Mine, S. Kagawa, *J. Phys. Chem.* 95 (1991) 3727.
- [2] R. Burch, *Catal. Rev. Sci. Eng.* 46 (2004) 271.
- [3] S. Brandenberger, O. Krocher, A. Tissler, R. Althoff, O. Kröcher, *Catal. Rev. Sci. Engg.* 50 (2008) 492.
- [4] J.H. Kwak, R.G. Tonkyn, D.H. Kim, J. Szanyi, C.H.F. Peden, *J. Catal.* 275 (2010) 187.
- [5] S.T. Korhonen, D.W. Fickel, R.F. Lobo, B.M. Weckhuysen, A.M. Beale, *Chem. Comm.* 47 (2011) 800.
- [6] W. Mortier, J. Pluth, J. Smith, *Mater. Res. Bull.* 12 (1977) 97.
- [7] D.W. Fickel, R.F. Lobo, *J. Phys. Chem. C* 114 (2010) 1633.
- [8] B.F. Mentzen, G. Bergeret, *J. Phys. Chem. C* 111 (2007) 12512.
- [9] U. Deka, A. Juhin, E.A. Eilertsen, H. Emerich, M.A. Green, S.T. Korhonen, B.M. Weckhuysen, A.M. Beale, *J. Phys. Chem. C* 116 (2012) 4809.
- [10] D. Klukowski, P. Balle, B. Geiger, S. Wagloehner, S. Kureti, B. Kimmerle, A. Baiker, *J.-D. Grunwaldt Appl. Catal. B* 93 (2009) 185.
- [11] G. Centi, S. Perathoner, *Appl. Catal. A* 132 (1995) 179.
- [12] J. Weitkamp, *Solid State Ionics* 131 (2000) 175.
- [13] G. Spoto, A. Zecchina, S. Bordiga, G. Ricchiardi, G. Martra, *Appl. Catal. B* 3 (1994) 151.
- [14] G. Spoto, S. Bordiga, D. Scarano, A. Zecchina, *C. Inorganica, C. Fisica, Catal. Lett.* 13 (1992) 39.
- [15] A.J. Hernández-Maldonado, R.T. Yang, *J. Am. Chem. Soc.* 126 (2004) 992.
- [16] L. Picone, S.J. Warrender, A.M.Z. Slawin, D.M. Dawson, S.E. Ashbrook, P.A. Wright, S.P. Thompson, L. Gaberova, P.L. Llewellyn, B. Moulin, A. Vimont, M. Daturi, P.M. Bum, S.S. Kyung, *Microporous Mesoporous Mater.* 146 (2011) 224.
- [17] T. Ishihara, M. Kagawa, F. Hadama, Y. Takita, *J. Catal.* 169 (1997) 93.
- [18] D.W. Fickel, E. D'Addio, J.A. Lauterbach, R. F. Lobo, *Appl. Catal. B*, 2011, 102, 441.
- [19] I. Bull, U. Muller, 2010, US Patent 0310440.
- [20] L. Ren, L. Zhu, C. Yang, Y. Chen, Q. Sun, H. Zhang, C. Li, F. Nawaz, X. Meng, *Chem. Comm.* 47 (2011) 9789.
- [21] J. Rodriguez-Carvajal, *Phys. C* 212 (1993) 259.
- [22] J. Rodriguez-Carvajal, *IUCr Newsletter* (1998) 35.
- [23] <http://www.iza-structure.org/databases>.
- [24] S.P. Thompson, J.E. Parker, J. Potter, T.P. Hill, A. Birt, T.M. Cobb, F. Yuan, C.C. Tang, *Rev. Sci. Instrum.* 80 (2009) 075107.
- [25] A.C. Larson, R.B. Von Dreele, *General Structure Analysis System (GSAS)* 748 (2000) 86.
- [26] S. Nikitenko, A.M. Beale, A.M.J. van der Eerden, S.D.M. Jacques, O. Leynaud, M.G. O'Brien, D. Detollenaere, R. Kaptein, B.M. Weckhuysen, W. Bras, *J. Sync. Rad.* 15 (2008) 632.
- [27] N. Binsted, EXCURV, CCLRC Daresbury Laboratory Computer, Program, 1998.
- [28] G. Centi, C. Nigro, S. Perathoner, G. Stella, *Catal. Today* 17 (1993) 159.
- [29] S.M. Jeong, S.H. Jung, K.S. Yoo, S.D. Kim, *Ind. Eng. Chem. Res.* 38 (1999) 2210.
- [30] S. Suarez, J. Martin, M. Yates, P. Avila, J. Blanco, *J. Catal.* 229 (2005) 227.
- [31] G. Delahay, B. Coq, S. Kieger, B. Neveu, *Catal. Today* 54 (1999) 431.
- [32] S. Kieger, G. Delahay, B. Coq, B. Neveu, *J. Catal.* 183 (1999) 267.
- [33] W. Arous, H. Tounsi, S. Djemel, A. Ghorbel, G. Delahay, *Surf. Sci.* 2005 (1883) 158.
- [34] W. Arous, H. Tounsi, S. Djemel, A. Ghorbel, G. Delahay, *Catal. Commun.* 6 (2005) 281.
- [35] M.H. Groothaert, K. Lievens, H. Leeman, B.M. Weckhuysen, R.A. Schoonheydt, *J. Catal.* 220 (2003) 500.
- [36] M.H. Groothaert, J.A. VanBokhoven, A.A. Battiston, B.M. Weckhuysen, R.A. Schoonheydt, *J. Am. Chem. Soc.* 125 (2003) 7629.
- [37] R. Vomscheid, M. Briend, M.J. Peltre, P.P. Man, D. Barthomeup, *J. Phys. Chem.* 98 (1994) 9614.
- [38] L. Maistriau, N. Dumont, J.B. Nagy, Z. Gabelica, E.G. Derouane, *Zeolites* 10 (1990) 243.
- [39] K.P. Lillerud, D. Akporiaye, *Stud. Surf. Sci. Catal.* 84 (1994) 543.
- [40] K. Kervinen, P.C.A. Bruijninx, A.M. Beale, J.G. Mesu, G. van Koten, R.J.M. Klien Gebbink, B.M. Weckhuysen, *J. Am. Chem. Soc.* 128 (2006) 3208.
- [41] J.G. Mesu, T. Visser, A.M. Beale, F. Soulimani, B.M. Weckhuysen, *Chem. Eur. J.* 12 (2006) 7167.
- [42] P. Frank, M. Benfatto, B. Hedman, K.O. Hodgson, *Inorg. Chem.* 47 (2008) 4126.
- [43] L.S. Kau, D.J. Spira-Solomon, J.E. Penner-Hahn, K.O. Hodgson, E.I. Solomon, *J. Am. Chem. Soc.* 109 (1987) 6433.
- [44] M. Sano, S. Komorita, H. Yamatera, *Inorg. Chem.* 31 (1992) 459.
- [45] S.M. Seo, W.T. Lim, K. Seff, *J. Phys. Chem. C* 116 (2012) 963.
- [46] O. Durá, R. Boada, A. Rivera-Calzada, C. Leon, E. Bauer, M.A. Lopez de la Torre, J. Chaboy, *Phys. Rev. B* 83 (2011) 045202.
- [47] V.F. Kispersky, A.J. Kropf, F.H. Ribeiro, J.T. Miller, *Phys. Chem. Chem. Phys.* 14 (2012) 2229.
- [48] M. Zmadacs, L. Kevan, *J. Phys. Chem.* 96 (1992) 8989.
- [49] W.B. Williamson, D.R. Flentge, J.H. Lunsford, *J. Catal.* 266 (1975) 258.
- [50] L. Gang, J.V. Grondelle, B.G. Anderson, R.A. van Santen, *J. Catal.* 109 (1999) 100.
- [51] D. Sen, N.H. Heo, H. Kang, K. Seff, *J. Phys. Chem. C* 115 (2011) 23470.